Dilepton low p_T suppression as an evidence of the Color Glass Condensate

M. A. Betemps* and M. B. Gay Ducati†
High Energy Physics Phenomenology Group, GFPAE
Instituto de Física, Universidade Federal do Rio Grande do Sul
Caixa Postal 15051, CEP 91501-970, Porto Alegre, RS, Brazil.
(Dated: February 7, 2008)

The dilepton production is investigated in proton-nucleus collisions in the forward region using the Color Glass Condensate approach. The transverse momentum distribution (p_T), more precisely the low p_T region where the saturation effects are expected to increase, is analyzed. The ratio between proton-nucleus and proton-proton differential cross section for RHIC and LHC energies is evaluated, showing the effects of saturation at small p_T, and presenting a suppression of the Cronin type peak at moderate p_T. These features indicate the dilepton as a most suitable probe to study the properties of the saturated regime and the Cronin effect.

PACS numbers: 11.15.Kc, 24.85.+p

I. INTRODUCTION

At high energies, the linear evolution equations, based in the standard perturbative QCD, predict a high gluon density, requiring that the growth of the parton density has to have a limit [1] - otherwise violation of the Froissart-Martin bound occurs - and expected to saturate at a scale Q_s, forming a color glass condensate (CGC)[2, 3, 4, 5]. In this context, the search for signatures of a CGC description of the saturated regime is an outstanding aspect of investigation in heavy ion colliders. The first results of Relativistic Heavy Ion Collider (RHIC), on charged hadron multiplicity in $Au-Au$ collisions, were treated considering that the CGC formulation gives a natural qualitative explanation of the data[6]. However, there are several issues to be clarified, before conclude that the dynamical of the partonic system should be described by a CGC already at RHIC energies. Particularly the current data are reasonably described by other models based on different assumptions [7, 8]. However, the charged multiplicity distribution in pseudo-rapidity for deuteron-gold collision is estimated within the CGC formalism at the deuteron fragmentation region, and pointed out as a probable signature of the saturated regime [9]. For a review of the CGC signatures see Refs. [10, 11].

In order to investigate the high energy limit of the partonic interactions, the proton-nucleus scattering was proposed as an ideal experiment to give evidences of the saturation effects described by the CGC in the proton fragmentation region [12, 13, 14]. Furthermore, the dilepton production was shown to be a sensitive probe of the perturbative shadowing and saturation dynamics in proton-proton, proton-nucleus and nucleus-nucleus scattering [15, 16, 17, 18, 19, 20, 21, 22, 23] in the forward kinematical region. It is an interesting observable since it is a clean process in which there is no strong interaction with the nuclear medium final state.

In this work we investigate quantitative features of the dilepton production in the forward region of proton-nucleus collisions in the context of the color glass condensate. In particular, the transverse momentum (p_T) distribution is studied focusing attention to the small p_T region, where the saturation effects are expected to be more significant. The main goal of this work is to show the effects of saturation at small p_T described by the CGC. Their presence at small p_T should be considered as a possible signature of the saturation effects when contrasted with proton-proton results. This comparison is performed evaluating the ratio between proton-nucleus and proton-proton cross section. This ratio shows two diferent behaviors; it presents Cronin type peak (if a local Gaussian for the correlator function is used) and a large suppression (if a non-local Gaussian is used), being a most suitable probe of the status of the Cronin effect as a final or initial state effect. This work is organized as follows. In the next section one presents a brief discussion on Color Glass Condensate formalism. In Sec. 3 the dilepton production cross section within the CGC formalism is presented. The Sec. 4 is devoted to the study on the color field correlator, which is a fundamental factor in the CGC approach. The numerical results are given and discussed in the last section where our conclusions are also presented.

II. THE COLOR GLASS CONDENSATE

The Color Glass Condensate picture holds in a frame in which the hadron propagates at the speed of light and, by Lorentz contraction, appears as an infinitesimally thin two-dimensional sheet located at the light cone. The formalism supporting this picture is in terms of a classical effective theory valid at small x region (large gluon density), and was originally proposed to describe the gluons in large nuclei [2].

At small x and/or large A one expects the transi-

*Electronic address: mandrebe@if.ufrgs.br
†Electronic address: gay@if.ufrgs.br

tion of the regime described by the standard perturbative QCD (Dokshitzer-Gribov-Lipatov-Altarelli-Parisi (DGLAP), Balitsky-Fadin-Kuraev-Lipatov (BFKL)) to a new regime where the processes like recombination of partons should be important in the parton cascade [1]. In this regime, the growth of the parton distribution is expected to saturate below a specific scale Q_s, forming a Color Glass Condensate [2, 3, 4, 5]. This saturated field, meaning the dominant field or gluons, has a large occupation number and allows the use of semi-classical methods. These methods provide the description of the small x gluons as being radiated from fast moving color sources (parton with higher values of x), being described by a color source density ρ_a, with internal dynamics frozen by Lorentz time dilatation, thus forming a color glass. The small x gluons saturate at a value of order $xG(x,Q^2) \sim 1/\alpha_s >> 1$ for $Q^2 \lesssim Q_s^2$, corresponding to a multi-particle Bose condensate state. The color fields are driven by the classical Yang-Mills equation of motion with the sources given by the large x partons. The large x partons move nearly at the speed of light in the positive z direction.

In the CGC approach the light cone variables are employed, where, $x^\mu \equiv (x^+, x^-, x_\perp)$, with $x^\pm \equiv 1/\sqrt{2}(x^0 \pm x^3)$ and $x_\perp \equiv (x^1, x^2)$, and $x^\mu p_\mu = x^+p^- + x^-p^+ - x_\perp \cdot p_\perp$. The variable x^+ is the time light cone, and p^- its variable conjugated identified with the energy as $p^- = \frac{(m^2+p_\perp^2)}{2p^+}$. The large x partons (fast) have momentum p^+, emitting (or absorbing) soft gluons with momentum $k^+ << p^+$, generating a color current only with the + component $J_a^+ = \delta(x^-)\rho_a$. In this framework, the nucleus is situated at $x^- \approx 0$, with an uncertainty $\Delta x^- \lesssim 1/k^+$, and there is a separation between fast and soft partons, implying that the former have large lifetime while soft partons have a short lifetime. These features assure that the color source density ρ_a should be considered time independent, since for the emitted soft gluons (small x gluons) the source is frozen in time. However, after a time interval of order $1/\varepsilon_p$ (ε_p being the energy of the source in the light-cone) the configuration of the source is different. In order to have a gauge-invariant formulation, the source ρ_a must be treated as a stochastic variable with zero expectation value. For these reason, an average over all configurations is required and it is performed through a weight function $W_{\Lambda^+}[\rho]$, which depends upon the dynamics of the fast modes, and upon the intermediate scale Λ^+, which defines fast ($p^+ > \Lambda^+$) and soft ($p^+ < \Lambda^+$) modes. The classical fields obey the Yang-Mills equation of motion,

$$D_\nu F_a^{\nu\mu}(x) = \delta^{\mu+}\rho_a(x^-, x_\perp), \tag{1}$$

and a physical observable is obtained by averaging the solution to this equation over all configurations of ρ_a, with the gauge-invariant weight function $W_{\Lambda^+}[\rho]$.

The effective theory is valid only at soft momenta of order Λ^+. Indeed, going to a much softer scale, there are large radiative corrections which invalidate the classical approximation. The modifications to the effective classical theory is governed by a functional, nonlinear, evolution equation, originally derived by Jalilian-Marian, Kovner, Leonidov and Weigert (JIMWLK) [3, 4] for the statistical weight function $W_{\Lambda^+}[\rho]$ associated with the random variable $\rho_a(x)$.

The solution for such functional evolution equation is not well determined yet and in order to make predictions or comparison with data, some phenomenological treatment should be given to the weight function. In this work an approximation to the weight function which is reasonable when we have large nuclei is used and consists in taking a Gaussian form [14, 24, 25]. As a consequence, most calculations in the CGC should be done quasi-analytically. In Ref. [24] it is shown that a Gaussian weight function can accommodate both the BFKL evolution of the gluon distribution at high transverse momenta, and the gluon saturation phenomenon at low transverse momenta. A non-local Gaussian distribution of color sources has been predicted in Ref. [26] as a mean-field asymptotic solution for the JIMWLK equation and provides some modifications concerning phenomenological properties of the observables [27]. The local Gaussian weight function assures that the color sources are correlated locally, on the other side, the non-local Gaussian allows correlations over large distances. In the following sections the phenomenological consequences of the choice of a local or non-local Gaussian type for the weight function are investigated concerning the transverse momentum of the dileptons.

III. DILEPTON PRODUCTION IN THE CGC APPROACH

At high energies, the dilepton production in hadronic collisions looks like a bremsstrahlung of a virtual photon with momentum $\mathbf{p}$ decaying into a lepton pair, which can occur before and after the interaction of the quark (momentum $\mathbf{k}$) with the dense saturated gluonic field (momentum $\mathbf{q}$) of the target, in our case the nucleus A. We consider only the diagrams where the photon emission occurs before and after before the interaction with the nucleus, since the emission considering before and after the interaction vanishes [28]. The dilepton production can be summarized in Figure 1 [16, 17, 21],

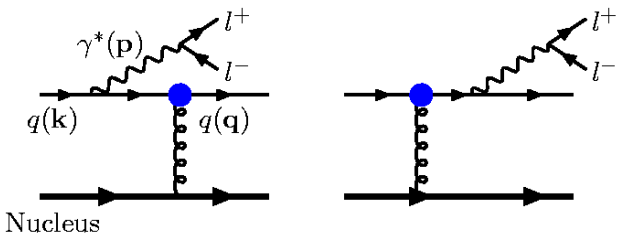

FIG. 1: Dilepton production in the CGC.

Considering the Fig. 1, the differential cross section

for the dilepton production in the CGC approach, for a collinear quark ($k_T = 0$), is written as [21],

$$\frac{d\sigma_{incl}^{qA\to ql^+l^-X}}{dz d^2p_T d\log M^2} = \pi R_A^2 f_q^2 \frac{2\alpha_{em}^2}{3\pi}\int \frac{d^2l_T}{(2\pi)^4} C(l_T)\left\{\left[\frac{1+(1-z)^2}{z}\right]\right.$$
$$\times \frac{z^2 l_T^2}{[p_T^2+M^2(1-z)][(p_T-zl_T)^2+M^2(1-z)]}$$
$$\left. - z(1-z)M^2\left[\frac{1}{[p_T^2+M^2(1-z)]} - \frac{1}{[(p_T-zl_T)^2+M^2(1-z)]}\right]^2\right\}, \quad (2)$$

where f_q represents the fraction of the electron charge carried by the quark q. The squared quark charge is $e_q^2 = f_q^2 e^2$ and the charge e^2 from e_q^2 was incorporated in the α_{em}^2 in the expression. R_A is the nuclear radius, $z \equiv p^-/k^-$ is the energy fraction of the proton carried by the virtual photon, p_T and M^2 are the transverse momentum and the squared invariant mass of the lepton pair, respectively; $l_T = q_T + p_T$ is the total transverse momentum transfer between the nucleus and the quark. The function $C(l_T)$ is the field correlator function and defined by [25],

$$C(l_T) \equiv \int d^2x_\perp e^{il_T\cdot x_\perp}\langle U(0)U^\dagger(x_\perp)\rangle_\rho, \quad (3)$$

with the averaged term representing the average over all configurations of the color fields in the nucleus, $U(x_\perp)$ is a matrix in the $SU(N)$ fundamental representation which represents the interactions of the quark with the classical color field. The correlator considers the two diagrams, being the interaction at two transverse locations, and all the information about the nature of the medium crossed by the quark is contained in the function $C(l_T)$. In particular, it determines the dependence on the saturation scale Q_s (and on energy).

In order to obtain a hadronic cross section, the validity of the collinear factorization in the fragmentation region is assumed and the expression in Eq. (2) is convoluted with the partonic distribution function in the proton (deuteron or nucleus), as was done in [17, 23] and the cross section reads as,

$$\frac{d\sigma^{pA\to ql^+l^-X}}{dp_T^2\, dM\, dx_F} = \frac{4\pi^2}{M} R_A^2 \frac{\alpha_{em}^2}{3\pi}\frac{1}{x_1+x_2}$$
$$\times \int \frac{dl_T}{(2\pi)^3}\; l_T\, W(p_T, l_T, x_1)\, C(l_T, x_2, A), \quad (4)$$

where x_F is the longitudinal momentum fraction given by $x_F = x_1 - x_2$, and x_1 and x_2 are the momentum fraction carried by the quark from the proton and by the gluonic field from the nucleus, respectively. The expression (4) is valid in the forward region, which means positive x_F, or positive rapidities y, and the variables x_1 and x_2 are defined by,

$$x_{\binom{1}{2}} = \frac{1}{2}\left\{\sqrt{x_F + 4\frac{M_T^2}{s}}(\pm)\, x_F\right\}, \quad (5)$$

or

$$x_{\binom{1}{2}} = \sqrt{\frac{M_T^2}{s}} e^{\pm y}, \quad (6)$$

where $M_T^2 = M^2 + p_T^2$ is the squared dilepton transverse mass and s is the squared center of mass energy. Here, using the structure function $F_2(x,Q^2) = \sum_i e_{q_i}^2 x[q_i(x,Q^2) + \bar{q}_i(x,Q^2)]$, the weight function $W(p_T, l_T, x_1)$ can be written as,

$$W(p_T, l_T, x_1) = \int_{x_1}^1 dz\, z F_2(x_1/z, M^2)$$
$$\times\left\{\frac{(1+(1-z)^2)z^2 l_T^2}{[p_T^2+M^2(1-z)][(p_T-zl_T)^2+M^2(1-z)]}\right.$$
$$- z(1-z)M^2\left[\frac{1}{[p_T^2+M^2(1-z)]}\right.$$
$$\left.\left. - \frac{1}{[(p_T-zl_T)^2+M^2(1-z)]}\right]^2\right\}. \quad (7)$$

In our calculations the CTEQ6L parametrization [29] was used for the structure function, and the lepton pair mass gives the scale for the projectile quark distribution. The function $W(p_T, l_T, x_1)$ plays the role of a weight function, selecting the regions of dominance on l_T contributing to the cross section.

In Eq. (4) the correlator function appears with an energy dependence (dependence on x_2), which is not included in the original McLerran-Venugopalan model. One includes such dependence in the field correlator function only in the saturation scale $Q_{s,A} \to Q_{s,A}(x)$ to simulate a low x evolution, as was done in the Ref. [27], in order to investigate the effects of the x evolution in the dilepton p_T spectra. The x dependence is parametrized in the form proposed by Golec-Biernat and Wüsthoff (GBW) [30] ($Q_s^2 = (x_0/x)^\lambda$), with the parameters taken

from the dipole cross section extracted from the fit procedure by GBW [30] and CGCfit [31] parametrizations, which will be discussed later.

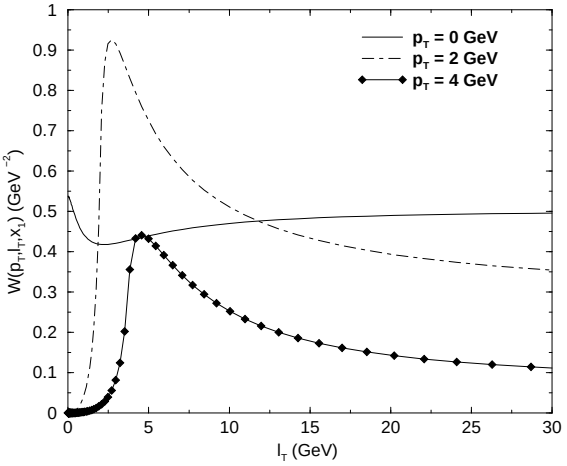

FIG. 2: Weight function for lepton pair mass $M = 3$ GeV and rapidity $y = 2.2$ versus l_T.

In Fig. 2, we plot the weight function for an specified lepton pair mass $M = 3$ GeV, in the forward region (positive x_F), with a positive value of the rapidity $y = 2.2$, considering the center of mass energy $\sqrt{s} = 350$ GeV (RHIC). In such figure the results for three representative values of p_T are presented, where a peak at $l_T \approx p_T$ and a suppression at $l_T < p_T$ are in order. These characteristics assure that the weight function selects the values of l_T larger than p_T. Moreover, one verifies that larger values of p_T provide a reduction in the normalization of the weight function at large values of l_T, when compared with the normalization at $p_T = 0$ GeV. This p_T behavior of the weight function is essential in order to determine the spectrum. As will be verified in the Sec. V, the p_T distribution is suppressed for large values.

All high density effects on the nucleus are encoded in the field correlator function. It is well known that the saturation effects in the correlator function $C(l_T, x, A)$ are present below the saturation scale, meaning the small l_T region (In the next section one observes this feature in the Fig. 3). Such behavior determines that only at small p_T the effects of saturation in the function $C(l_T, x, A)$ should be measurable, once the weight function selects the values of l_T larger than p_T.

To make a quantitative prediction to the dilepton production, the correlator function $C(l_T, x, A)$ has to be determined. It plays an important role in the Color Glass Condensate formalism and should be compared with the dipole cross section. It is related to dipole Fourier transform and in the following, the function $C(l_T, x_2, A)$ will be discussed, through the analyses of some phenomenological models.

IV. THE COLOR FIELD CORRELATOR $C(l_T, x, A)$

The function $C(l_T)$ is considered a fundamental quantity in the CGC formalism, since it contains all the information on high density effects. It can be related to the Fourier transform (F.T.) of the dipole cross section in the following way [22, 32, 33],

$$C(l_T) = \frac{1}{\sigma_0}\int d^2x_\perp e^{il_T\cdot x_\perp}[\sigma_{dip}(x_\perp \to \infty) - \sigma_{dip}(x_\perp)], \quad (8)$$

where σ_0 is the normalization of the dipole cross section at the saturation region ($x_\perp \to \infty$). Considering the GBW model for the dipole cross section $\sigma_{dip}(x_\perp, x) = \sigma_0[1-\exp(-Q_s^2(x)x_\perp^2/4)]$ [30] the correlator function can be written as [22, 33],

$$C(l_T, x, A)_{GBW} = \frac{4\pi}{Q_s^2(x,A)} e^{-\frac{l_T^2}{Q_s^2(x,A)}}, \quad (9)$$

where a simple dependence on energy (x) and atomic number (A) was taken into the saturation scale. Namely, the nuclear saturation scale was considered as $Q_s^2(x, A) = A^{1/3}Q_s^2(x)$ with $Q_s^2(x)$ being the proton saturation scale parametrized of the form proposed by GBW $Q_s^2 = (x_0/x)^\lambda$ [30], where the parameters $x_0 = 3.10^{-4}$ and $\lambda = 0.288$ were determined from the fit to the Hadron Electron Ring Accelerator (HERA) data. This ansatz to the nuclear dependence of the saturation scale was studied in the Ref. [34] concerning the eA data, and was shown to be a consistent approximation for large nuclei and moderate energies.

However, the GBW F.T. (Eq. (9)) does not recover the perturbative behavior at large p_T, since it presents an exponential tail, as we show in the Fig. 3.

Considering the McLerran-Venugopalan (MV) model, the function $C(l_T)$ has no energy dependence and should be computed by taking the MV dipole cross section [22],

$$\sigma_{dipole}(r_\perp) = \pi R^2\left[1 - e^{\left(-\frac{Q_s^2}{\pi}\int\frac{dp}{p^3}(1-J_0(pr_\perp))\right)}\right]. \quad (10)$$

The Fourier transform can be numerically computed in the form [25],

$$C(l_T)_{MV} \equiv \int d^2x_\perp e^{il_T\cdot x_\perp} e^{-\frac{Q_s^2}{\pi}\int\frac{dp}{p^3}(1-J_0(px_\perp))}, \quad (11)$$

where the value of Q_s^2 is fixed depending on the energy. However, no x evolution is presented in the MV model and the energy dependence is introduced in the correlator by fixing the value of the saturation scale. Following the equation (11), we propose to introduce the dependence on the energy and nuclei into the saturation scale in the form,

$$C_{MV_{mod}}(l_T, x, A) = \int d^2x_\perp e^{il_T\cdot x_\perp} \times e^{-\frac{Q_s^2(x,A)}{\pi}\int\frac{dp}{p^3}(1-J_0(px_\perp))}. \quad (12)$$

The nuclear saturation scale is parametrized in the form presented previously, where the x dependence in the saturation scale $Q_s^2(x)$ is considered from the parameters extracted from the fit to HERA data and should be taken from GBW saturation model [30], or from a dipole cross section based on the CGC approach [31]. Here it should be interesting to point out that in the recent work of Ref. [27], the Cronin effect was studied in the MV model, and the same energy dependence for the saturation scale was considered. Such a simple inclusion of the quantum corrections results in a disagreement with the RHIC $d-Au$ data at forward rapidities concerning the Cronin effect [35, 36]. In that work [27], a non-local Gaussian distribution for $\langle U^\dagger(0)U(x_\perp)\rangle$ was introduced and the shape of the curves agrees with the Broad Range Hadron Magnetic Spectrometer (BRAHMS) data at large rapidities, however presents large suppression at central rapidity. This disagreement shows that the dynamics of the CGC is a subject which deserves more comprehensive studies. Here we point out that the dilepton transverse momentum analyzed with local and non-local Gaussian correlator is a good observable to investigated such dynamics.

In the large l_T ($l_T >> Q_s$) limit, the correlator function should recover the perturbative behavior ($1/l_T^4$), and considering the MV model the correlator function can be expanded and written in a simple analytic expression [25],

$$C_{MV_{mod}}(l_T,x,A)|_{l_T>>Q_s} = 2\frac{Q_s^2(x,A)}{l_T^4} \times \left(1+\frac{4Q_s^2(x,A)}{\pi l_T^2}\left[\ln\left(\frac{l_T}{\Lambda_{QCD}}\right)-1\right]\right), \quad (13)$$

which emphasizes the large saturation effects in the small l_T region, as in the Fig. (3).

In a recent work, Ref. [31] it has been analyzed the structure function $F_2(x,Q^2)$ for $x<10^{-2}$ and $0.045 \leq Q^2 \leq 45$ GeV^2, within the dipole picture, taking an expression to the dipole cross section which interpolates the BFKL solution at $r << 1/Q_s(x)$ and the saturated behavior at $r >> 1/Q_s(x)$, where the scattering amplitude saturates at one. The parametrized dipole cross section can be written as $\sigma_{dip}(x,r) = 2\pi R^2 \mathcal{N}(rQ_s,x)$ with [31],

$$\begin{aligned} \mathcal{N}(rQ_s,Y) &= \mathcal{N}_0\left(\frac{rQ_s}{2}\right)^{2\left(\gamma_s+\frac{\ln(2/rQ_s)}{\kappa\lambda Y}\right)} \quad \text{to} \quad rQ_s \leq 2 \\ \mathcal{N}(rQ_s,Y) &= 1-e^{-a\ln^2(brQ_s)} \quad \text{to} \quad rQ_s \geq 2, \end{aligned} \quad (14)$$

where $Y=\ln(1/x)$. There are three free parameters: the proton radius R, the value x_0 of x at which the saturation scale has to be equal to 1, and the parameter which controls the energy dependence of the saturation scale λ. The parameters a and b are determined to assure that $\mathcal{N}$ is continuous at $rQ_s=2$ (at least at first derivative). From the fit to the HERA data for the inclusive structure function $F_2(x,Q^2)$ the parameters depend on the quark mass m_q.

Following this dipole cross section, we construct a function $C(l_T,x_2,A)$ taking the Eq. (8), that will be called CGCfit, and obtain the following expression,

$$\begin{aligned} C(l_T,x,A)_{CGC} &= 2\pi\left(\int_0^{2/Q_s} rdrJ_0(l_Tr)\left(1-\mathcal{N}_0\exp\left\{2\ln\left(\frac{rQ_s}{2}\right)\left[\gamma_s+\frac{\ln(2/rQ_s)}{\kappa\lambda\ln 1/x}\right]\right\}\right)\right. \\ &+ \left.\int_{2/Q_s}^{\infty} rdrJ_0(l_Tr)e^{-a\ln^2(brQ_s)}\right). \end{aligned} \quad (15)$$

The energy and nuclear dependences are introduced with $Q_s^2(x,A) = A^{1/3}\left(\frac{x_0}{x}\right)^\lambda$.

Considering the two models for the dipole cross section (GBW and CGCfit) there is a set of parameters which determine the saturation scale, where the ones used in this work are presented in the Table I (the set of parameters are identified as fit1, fit2 and fit3), where the value of the saturation scale was calculated at $x=10^{-3}$ for gold. It is shown that the recent CGC fit parameters provide a small value for the saturation scale, and this behavior should affect the dilepton production, as we will see in the next section. The nuclear radius is taken from the Woods-Saxon parametrization of the form, $R_A = 1.2A^{1/3}fm$, while the proton radius is taken from the fits and presented in the Table I.

In the Figure 3 the function $C(l_T,x_2,A)$ is shown for the models discussed here and one verifies the large saturation effects at small l_T when we compare the functions obtained from the GBW and CGCfit with the asymp-

Parameter	GBW (fit1)	CGC fit $m_q = 10$ MeV (fit2)	CGC fit $m_q = 140$ MeV (fit3)
x_0	3×10^{-4}	1.06×10^{-4}	0.267×10^{-4}
λ	0.288	0.285	0.253
Q_s^2 ($x = 10^{-3}$, $A = 197$)	4.114 GeV^2	3.069 GeV^2	2.327 GeV^2
R_p (Proton radius)	0.6055 fm	0.566 fm	0.641 fm

TABLE I: Parameters of saturation scale from GBW and CGCfit.

totic behavior of the correlator function. At this point it is interesting to emphasize some features of the functions $C(l_T, x_2, A)$ extracted from the Fourier transform of GBW dipole cross section and the Fourier transform of the CGCfit. Considering the GBW F.T. (dashed-line) the function $C(l_T, x_2, A)_{GBW}$ depends on $e^{-l_T^2}$ and is suppressed at large l_T (this behavior is shown in the inner plot on Fig. 3). It results in an unrealistic suppression of the observable cross section at large p_T, as emphasized in the Refs. [22, 33]. Considering the results from CGC fit (solid-line), the function $C(l_T, x_2, A)$ presents negative values at moderate l_T (as can be seen in the Figure 3) and this behavior should be due to the continuity only at first derivative or by the approximations in the construction of the dipole cross section model [31]. Having those aspects in mind, the function $C(l_T, x_2, A)$ based on the McLerran-Venugopalan model, including an energy and nuclear dependence in the saturation scale, is employed here. The parameters to the saturation scale are taken from the fit1 (triangle-up-line) and fit2 (circle-line) and one verifies in the Fig. 3 that the value of the saturation scale provides a small difference in the correlator obtained from the MV$_{mod}$ model at small l_T.

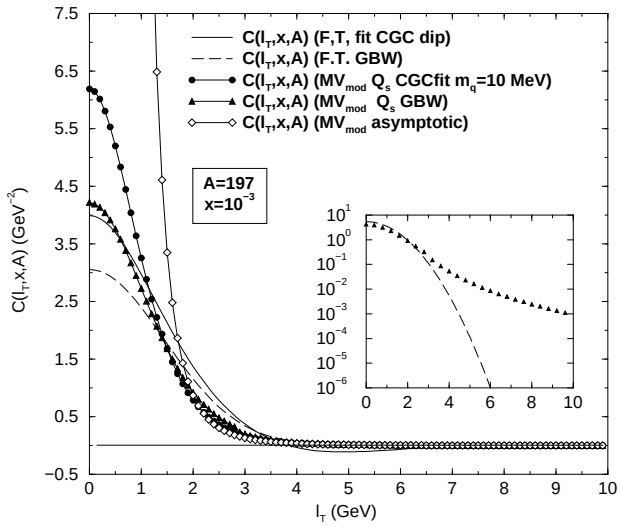

FIG. 3: Correlator $C(l_T, x, A)$ as a function of l_T.

The correlator function is suppressed at large l_T, and the weight function suppress the values of l_T smaller than p_T, the behavior of the cross section coming from the balance between these two quantities. In such balance, the small p_T dileptons clearly are the dominant contribution for the cross section and provide a physical probe for the CGC and for the models to the color field correlator function.

The field correlator function presented up to here in MV model is obtained considering a local Gaussian function for the weight function $W_{\Lambda^+}[\rho]$. The correlator function is defined by

$$C(l_T) \equiv \int d^2x_\perp e^{il_T\cdot x_\perp} \langle U(0)U^\dagger(x_\perp)\rangle_\rho, \qquad (16)$$

and the local Gaussian enters in the calculation of the averaged term $\langle U(0)U^\dagger(x_\perp)\rangle_\rho$. The consideration of a non-local Gaussian function modifies the correlator in such way that it is written as [24, 27]

$$C(l_T, x, A) \equiv \int d^2x_\perp e^{il_T\cdot x_\perp} e^{\chi(x, x_\perp, A)}, \qquad (17)$$

with

$$\chi(x, x_\perp, A) \equiv -\frac{2}{\gamma c}\int \frac{dp}{p}(1 - J_0(x_\perp p)) \times \ln\left(1 + \left(\frac{Q_2^2(x, A)}{p^2}\right)^\gamma\right), \qquad (18)$$

where, γ is the anomalous dimension ($\gamma \approx 0.64$ for BFKL) and $c \approx 4.84$ [24, 27]. This non-local field correlator function is plotted in the Figure 4 in contrast with the same correlator obtained with the local Gaussian weight functional.

The physical effect of the nonlocal Gaussian weight function is that the gluon sources are no longer correlated locally, as in the local Gaussian, but correlate over larger distances. This implies in a more drastic reduction of the gluon density, as can be seen at small l_T in the Fig. 4, where the solid line represents the correlator function with a local Gaussian weight function and the long-dashed line represents the non-local Gaussian weight function. The effect of the local or non-local Gaussian weight function in the p_T dilepton spectra will be discussed in the next section in the context of the defined ratio R_{pA}.

Having addressed all the fundamental aspects to develop the calculation of the dilepton transverse momentum in the CGC formalism, one presents in the next section the numerical predictions using such approach and the discussions.

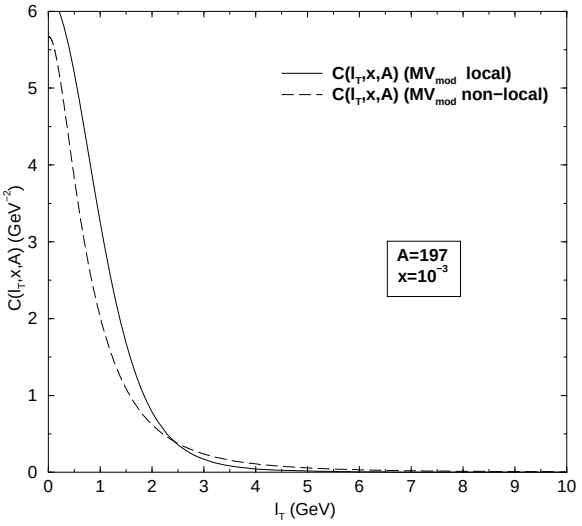

FIG. 4: Field correlator function with local and non-local Gaussian weight function.

V. RESULTS AND DISCUSSIONS

In what follows, the numerical results on the dilepton transverse momentum distribution in CGC are addressed and discussed. We consider pA collisions at RHIC ($\sqrt{s} = 350$ GeV) and LHC energies ($\sqrt{s} = 8.8$ TeV) in the proton fragmentation region (positive rapidities). The calculations are performed fixing values of rapidities (or x_F) and lepton pair mass M. We use the function $C(l_T, x_2)$ based on the McLerran-Venugopalan model, however an x dependence through the saturation scale is introduced, taking the parameters from the HERA data fit procedure GBW (fit1) [30] and CGCfit (fit2) [31]. For sake of comparison, the same differential cross section using the original McLerran-Venugopalan model, fixing a value to the saturation scale is evaluated.

In Fig. 5 we present the transverse momentum distribution for RHIC energies ($\sqrt{s} = 350$ GeV) in pA collisions, for a lepton pair mass $M = 3$ GeV and as in the Ref. [23] at rapidity $y = 2.2$. The proton structure function is taken from the CTEQ6L parametrization [29]. The solid line is the calculation with the McLerran-Venugopalan model, with the x dependence on the saturation scale, taking the parameters from the fit2; the dashed-line is the same calculation with the saturation scale taken from the fit1 and the dot-dashed line is the calculation with the asymptotic behavior of the MV correlator function. Considering the transverse momentum distribution at fixed mass and rapidities, the effects of quantum evolution are not too relevant in the range of transverse momentum investigated here, once the parametrization of the saturation scale assures that it is almost fixed in the region treated in this case, changing only weakly with the transverse momentum ($x_2 = \sqrt{\frac{M^2+p_T^2}{s}}e^{-y}$). Such behavior can be seen in the Figs. 5 and 6, where the line-diamond represents the calculation with the MV model, fixing the saturation scale at a value $Q_s^2 = 3.2$ GeV ^{2} and $Q_s^2 = 8$ GeV^2, respectively. The x evolution provides a small suppression of the large p_T dilepton, in both cases.

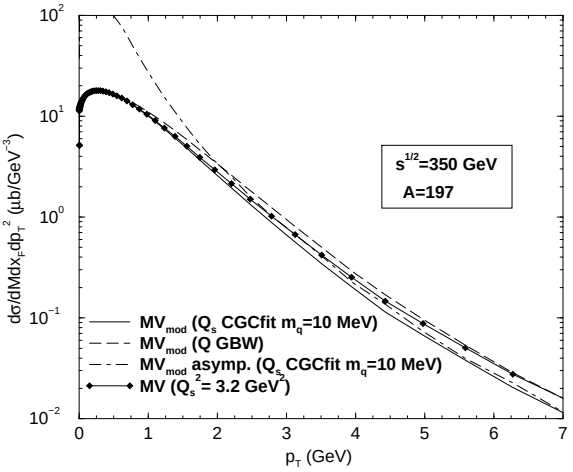

FIG. 5: Dilepton production at RHIC energies ($\sqrt{s} = 350$ GeV) in pA collisions, considering rapidity $y = 2.2$ and lepton pair mass $M = 3$ GeV.

In the Figure 5 the large saturation effects presented at $p_T \lesssim 2$ GeV are verified if one compares the asymptotic behavior of the correlator function with the MV$_{mod}$ prediction. As was shown in the last section, the asymptotic behavior of the correlator function ($l_T >> Q_s$) depends on the Q_s^2/l_T^4, then an increase of the saturation scale provides an increase in the differential cross section at large p_T, as can be seen in the Figure 5. As a most interesting feature, only at large p_T the effects of the choice of saturation scale affect the cross section, and the difference between the predictions being a factor of 2 considering the smallest value of the saturation scale, which is taken from the fit3, in contrast with the GBW ones.

In Figure 6 the dilepton transverse momentum distribution at LHC energies is shown, taking the same value of rapidity $y = 2.2$ to assure the forward region and to make a comparison with RHIC energies. The same behavior concerning the saturation effects is verified, although such effects start to be significant for $p_T \lesssim 4$ GeV. The estimative with the MV model was performed and the suppression at large p_T when the energy dependence is introduced in the saturation scale can be seen. The p_T spectra is enlarged at large p_T if the saturation scale is large, as was verified for RHIC energies.

In order to avoid any ambiguity with normalization, the ratio between the proton-nucleus and proton-proton differential cross section for RHIC and LHC is defined,

$$R_{pA} = \frac{\frac{d\sigma(pA)}{\pi R_A^2 dM dx_F dp_t^2}}{A^{1/3}\frac{d\sigma(pp)}{\pi R_p^2 dM dx_F dp_t^2}}. \qquad (19)$$

Some attention should be given to the uncertainty in the

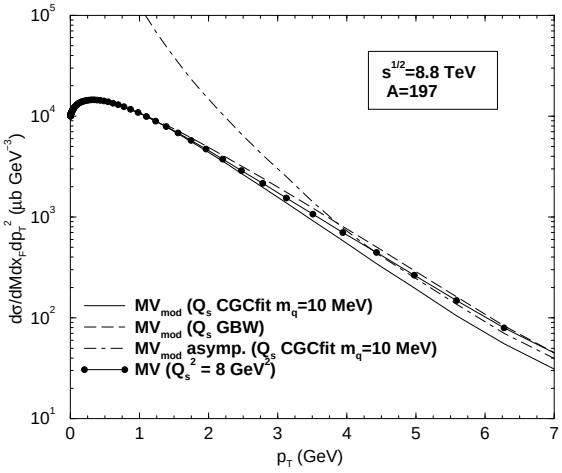

FIG. 6: Dilepton production at LHC energies ($\sqrt{s} = 8.8$ TeV) in pA collisions, considering rapidity $y = 2.2$ and lepton pair mass $M = 3$ GeV.

determination of the nuclear radius, then each cross section is divided by the nuclear or proton radius. The factor $A^{1/3}$ was used in the denominator to guarantee a ratio R_{pA} about 1 at large p_T.

The expression to the ratio R_{pA} in the dilepton production defined here should be written of the form,

$$R_{pA} \quad (y, p_T) = \frac{\int d^2 l_T W(p_T, l_T, x_1) C_A(l_T, x_2, A)}{A^{1/3} \int d^2 l_T W(p_T, l_T, x_1) C_p(l_T, x_2)}, \qquad (20)$$

where C_A is the nuclear correlator function and C_p is the proton correlator function. The ratio in the Eq. (20) is similar to the one obtained in the Ref. [27] to investigate the Cronin effect (Eq. (113) in the Ref. [27]).

The Cronin effect was discovered in the late's 70s [37] and is related to the enhancement of the hadron transverse momentum spectra at moderated p_T (2-5 GeV) in comparison with the proton-proton collisions (the ratio between pA and pp present a peak at moderate p_T). The effect should be interpreted as being originated by the multiple scatterings of the partons from the proton propagating through the nucleus, resulting in a broadening of the transverse momentum of the initial partons. This indicates the Cronin effect as an initial state effect. The Cronin effect was measured by the RHIC experiments, in $Au - Au$ and $d - Au$ collisions, however, the theoretical approaches cannot describe the effect in all the range of rapidity measured by the collaborations [38]. Although the Cronin effect concerns the hadron transverse momentum spectra, it is also expected in the dilepton transverse momentum spectra, since the effect of multiple scatterings is an initial state effect. Moreover, the ratio obtained in this work is similear to that is used to investigate the Cronin effect [27].

In the Fig. (7) one presents the results for the ratio R_{pA} to RHIC and LHC energies considering a correlator field function $C(l_T, x, A)$ obtained from a local Gaussian distribution for the weight function $W_{\Lambda^+}[\rho]$. For RHIC energies the solid line represents the calculation for rapidity $y = 2.2$ and the dashed line for rapidity $y = 3.2$. For LHC energies the long-dashed line represents the calculation for rapidity $y = 2.2$ and the dot-dashed line for rapidity $y = 3.2$. It is verified that at moderate p_T the calculations show a Cronin type peak for RHIC and for LHC (there is a suppression of the dilepton production at RHIC and LHC energies comparing with the proton-proton collisions at small p_T, at intermediate p_T the ratio is larger than 1, and there is a suppression at large p_T up to get the value 1). Such peak increases and is shifted to larger p_T at larger rapidities, due to the fact that the saturation scale grows with the rapidity and no evolution is taking into account.

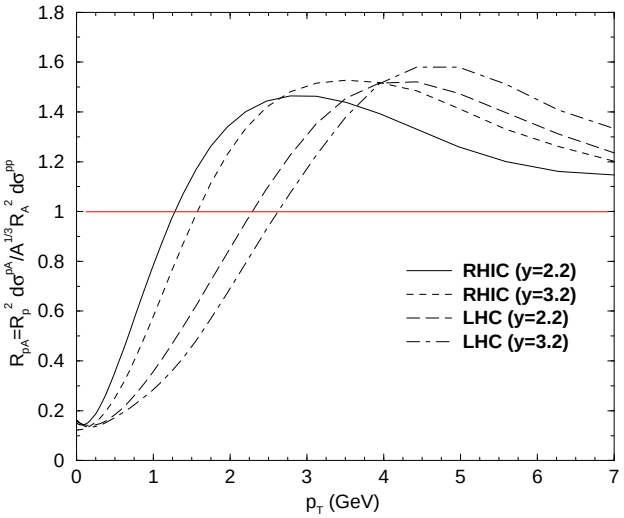

FIG. 7: Ratio between proton-nucleus and proton-proton at RHIC and LHC energies by the CGC approach at distincts rapidities with local Gaussian distribution for the weight function $W[\rho]$.

Concerning the Cronin effect, such peak is enlarged at large rapidities if the local Gaussian correlator function with the same energy dependence implemented here is used [27], in complete disagreement with the BRAHMS experiment at forward rapidities [35, 36]. In the same Ref. [27] the Cronin effect was studied using a non-local Gaussian distribution for the weight function and the Cronin peak suppression is reached. However, there is a suppression on the normalization at centrality region, which is not consistent with the RHIC data in central rapidity [35, 36], emphasizing that the the non-local Gaussian weight function should be the right physics at forward rapidities.

On the dilepton side, the behavior of the ratio R_{pA}, shows the same features of the Cronin peak at forward rapidities when investigated with the local Gaussian (the peak is enlarged and shifted to high p_T at large rapidities). However, the ratio R_{pA} was also investigated with the correlator function obtained from a non-local Gaus-

sian weight function $W_{\Lambda^+}[\rho]$, and is presented in the Fig. 8. The suppression of the ratio R_{pA} is verified showing exactly the same features presented in the Cronin effect [27], being a possible clean observable to study this property. Although, the Cronin effect was considered as a final state one in the Ref. [39], in our analysis, the dilepton production seems to clarify this aspect. It was obtained that the Cronin type peak (or the suppression of the Cronin peak) in the dilepton p_T distribution appears as an initial state effect. In the Fig. (8) the solid line represents the calculation for rapidity $y = 2.2$ and the dashed line for rapidity $y = 3.2$ at RHIC energies. For LHC energies the long-dashed line represents the calculation for rapidity $y = 2.2$ and the dot-dashed line for rapidity $y = 3.2$.

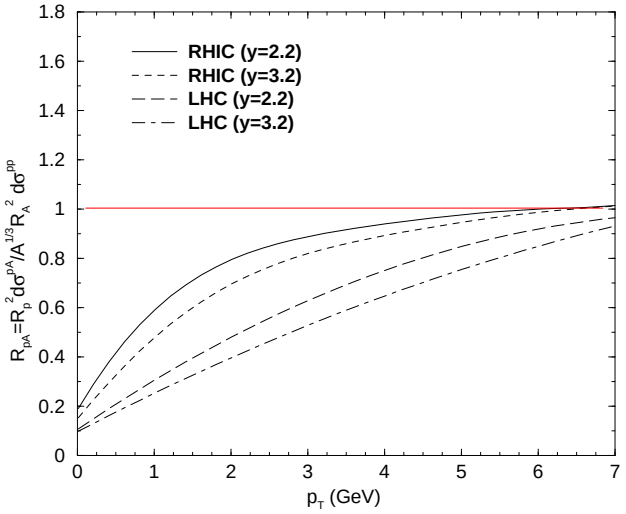

FIG. 8: Ratio between proton-nucleus and proton-proton at RHIC and LHC energies by the CGC approach at distincts rapidities with non-local Gaussian distribution for the weight function $W[\rho]$.

At RHIC energies, the effect of suppression appears if the nonlocal Gaussian in the correlator color field is used, sugesting the measurement of such suppression, although the detectors should not be able to measure such behavior [40]. On the other hand, at LHC energies, the suppression of the ratio R_pA reach large values of p_T and such suppression increases with the rapidity. It is interesting to address that at LHC the experimental facilities provide a detection of dileptons in the forward region with transverse momentum above 1.5 GeV, depending on the rate of the signal of the observable and on the signal from physics and machine sources [41]. This feature assures that at LHC energies such suppression behavior should be detectable too.

VI. CONCLUSIONS

In this work the large saturation effects described by the Color Glass Condensate in the dilepton production at small p_T region and the dependence of the large p_T spectra on the saturation scale value are verified. Although at RHIC, the transverse momentum distribution of the dilepton should not be measurable in the very small p_T, at intermediate p_T, the comparison between pp and pA cross section, provides a tool to study the Cronin effect and the dynamics of the Color Glass Condensate.

Particularly, the dilepton transverse momentum distribution presents the suppression of the Cronin type peak, as observed in the inclusive observables, if a non-local Gaussian is used. Such behavior is observed in the Fig. (8). At the LHC energies, at forward rapidities, the effect of suppression increases (Fig. (8)). Such large suppression at high energies gives an indication that dilepton transverse momentum provides a clear probe of the Color Glass Condensate description of the high energy hadronic interactions in the forward rapidity region. Moreover, the dilepton p_T spectra should be used to investigate the properties of the Cronin effects and indicates it as an initial state effect. Our results confirm the studies of Refs. [17, 18, 20] concerning the saturation effects. In addition to this analysis, in a recent work [19], the high p_T and low mass region in the dilepton production in perturbative QCD with all-order resummation was pointed as a good probe of the gluon distribution, as was indicated in the Refs. [15] considering the dipole approach. Also, the mass distributions of the dileptons investigated in the CGC should identify effects of saturation at small mass region [23]. The ensemble of these features shows that dilepton production is an observable that deserves to be measured, once it carries information about the high density nuclear system.

Acknowledgments

We would like to thank L. McLerran, E. Iancu and R. Venugopalan for discussions during the IX Hadron Physics held in Brazil, K. Safarik for the elucidating comments on experimental features of the muon detector at LHC, M. V. T. Machado for useful comments, and F. Gelis for the comments about Fourier transform of the CGC fit dipole cross section, for providing a code to evaluate quickly the Fourier transform integrals and by a careful reading of this manuscript. This work was supported by CNPq, Brazil.

[1] L. V. Gribov, E. M. Levin, M. G. Ryskin, *Phys. Rep.* 100, 1 (1983).
A. H. Mueller, J. W. Qiu. *Nucl. Phys. B*268, 427 (1986).
A. H. Mueller, *Nucl. Phys. B*335, 115 (1990).
A. H. Mueller, *Nucl. Phys. B*558, 285 (1999).
A. L. Ayala, M. B. Gay Ducati, E. M. Levin, *Nucl. Phys.*

*B*493, 305 (1997); A. L. Ayala Filho, M. B. Gay Ducati, and E. M. Levin, ibid. 511, 355 (1998).
[2] L. McLerran, R. Venugopalan, *Phys. Rev. D*49, 2233 (1994); *ibid.* 49, 3352 (1994).
[3] J. Jalilian-Marian., A. Kovner, A. Leonidov, H. Weigert, *Nucl. Phys. B*504, 415 (1997); *Phys. Rev. D*59, 014014 (1999).
[4] E. Iancu, A. Leonidov, L. D. McLerran, *Nucl. Phys. A*692, 583 (2001); *Phys. Lett. B*510, 133 (2001);
[5] E. Ferreiro, E. Iancu, A. Leonidov, L. McLerran, *Nucl. Phys. A*703, 489 (2002).
[6] D. Kharzeev, M. Nardi, *Phys. Lett. B*507, 121 (2001).
D. Kharzeev, E. Levin, *Phys. Lett. B*523, 79 (2001).
D. Kharzeev, E. Levin, L. McLerran, *Phys. Lett. B*561, 93 (2003).
[7] K. J. Eskola, *Nucl. Phys. A*698, 78 (2002).
[8] N. Armesto, C. Pajares, *Int. J. Mod. Phys. A*15, 2019 (2000).
[9] D. Kharzeev, E. Levin, M. Nardi, *Nucl. Phys. A*730, 448 (2004). Erratum-ibid. 743, 329 (2004).
[10] J.P. Blaizot, F. Gelis, ePrint arXiv:hep-ph/0405305.
[11] L. McLerran, ePrint arXiv:hep-ph/0402137.
[12] Y. V. Kovchegov, A. H. Mueller, *Nucl. Phys. B*529, 451 (1998).
[13] A. Dumitru, L. McLerran, *Nucl. Phys. A*700, 492 (2002).
[14] E. Iancu and R. Venugopalan, ePrint arXiv:hep-ph/0303204.
[15] M.A. Betemps, M.B. Gay Ducati, M.V.T. Machado, *Phys. Rev. D*66, 014018 (2002);
M.A. Betemps, M.B. Gay Ducati, M.V.T. Machado, J. Raufeisen, *Phys. Rev. D*67, 114008 (2003).
[16] B.Z. Kopeliovich, In proceedings *Workshop Hirschegg'95: Dynamical Properties of Hadrons in Nuclear Matter.* Ed. by H. Feldmeier and W. Nörenberg, GSI, Darmstadt, p. 102 (1995) [hep-ph/9609385];
S.J. Brodsky, A. Hebecker, E. Quack, *Phys. Rev. D*55, 2584 (1997).
[17] B. Z. Kopeliovich, J. Raufeisen, A. V. Tarasov, *Phys. Lett. B*503, 91 (2001).
[18] B. Z. Kopeliovich, J. Raufeisen, A. V. Tarasov, M. B. Johnson, *Phys. Rev. C*67, 014903 (2003).
[19] G. Fai, J. w. Qiu and X. f. Zhang, it J. Phys. G 30, S1037 (2004).
[20] R. Baier, A. H. Mueller, D. Schiff, *Nucl. Phys. A*741, 358 (2004).
[21] F. Gelis, J. Jalilian-Marian, *Phys. Rev. D*66, 094014 (2002).
[22] F. Gelis, J. Jalilian-Marian, *Phys. Rev. D*67, 074019 (2003).
[23] J. Jalilian-Marian, *Nucl. Phys. A*739, 319 (2004).
[24] E. Iancu, K. Itakura, L. McLerran, *Nucl. Phys. A* 724, 181 (2003).
[25] F. Gelis, A. Peshier, *Nucl. Phys. A*697, 879 (2002).
[26] E. Iancu, A. Leonidov and L. D. McLerran, *Phys. Lett. B*510, 133 (2001).
[27] J.P. Blaizot, F. Gelis, R. Venugopalan, *Nucl. Phys. A*743, 13 (2004).
[28] F. Gelis and J. Jalilian-Marian, *Phys. Rev. D*66, 014021 (2002).
[29] J. Pumplin, D.R. Stump, J. Huston, H.L. Lai, P. Nadolsky, W.K. Tung, JHEP 0207, 012 (2002).
[30] K. Golec-Biernat, M. Wüsthoff, *Phys. Rev. D*59, 014017 (1999). *ibid.* 60, 114023 (1999). *idem Eur. Phys. J* C20, 313 (2001).
[31] E. Iancu, K. Itakura, S. Munier, *Phys. Lett. B*590, 199 (2004).
[32] J. Bartels, K. Golec-Biernat, H. Kowalski, *Phys. Rev. D*66, 014001 (2002).
[33] V. P. Gonçalves, M. V. T. Machado, *Eur. Phys. J. C*31, 371 (2003).
[34] A. Freund, K. Rummukainen, H. Weigert, A. Schäfer, *Phys. Rev. Lett.* 90, 222002 (2002).
[35] BRAHMS collaboration, R. Debbe, *J. Phys. G*30, S759 (2004).
[36] BRAHMS collaboration, I. Arsene *et al.*, arXiv:nucl-ex/0403005.
[37] J. W. Cronin *et al.*, *Phys. Rev. D*11, 3105 (1975).
[38] A. Accardi, ePrint arXiv:nucl-th/0405046.
[39] R. C. Hwa, C. B. Yang, *Phys. Rev. Lett.* 93, 082302 (2004).
[40] K. Adcox et al., *Phys. Rev. Lett.* 88, 192303 (2002).
[41] ALICE Collaboration, CERN/LHCC-99-22, Aug. 1999.; K. Safarik, private communication.